UltraShiver: Lateral Force Feedback on a Bare Fingertip via Ultrasonic Oscillation and Electroadhesion

Heng Xu, *Member, IEEE*, Michael A. Peshkin, *Senior Member, IEEE*, and J. Edward Colgate, *Fellow, IEEE*

***Abstract*—We propose a new lateral force feedback device, the UltraShiver, which employs a combination of in-plane ultrasonic oscillation (around 30 kHz) and out-of-plane electroadhesion. It can achieve a strong active lateral force (400 mN) on the bare fingertip while operating silently. The lateral force is a function of pressing force, lateral vibration velocity, and electroadhesive voltage, as well as the relative phase between the velocity and voltage. In this paper, we perform experiments to investigate characteristics of the UltraShiver and their influence on lateral force. A lumped-parameter model is developed to understand the physical underpinnings of these influences. The model with frequency-weighted electroadhesion forces shows good agreement with experimental results. In addition, a Gaussian-like potential well is rendered as an application of the UltraShiver.**

***Index Terms*—Surface haptics, lateral force feedback, active force, ultrasonic oscillation, electroadhesion.**

I. Introduction

Among haptic rendering technologies, lateral forces between the human fingertip and an object's surface play an important role in creating the illusion of texture and shape perception. By modulating the lateral friction force, spatial friction maps of physical textures can be generated [1]–[4] and the profile gradient of a 2.5D shape can be approximately matched [5]–[7].

There are two methods to modulate the friction force: ultrasonic friction reduction (what we call the TPaD) [1], [8] and electroadhesive attraction [2], [3], [9]. Ultrasonic friction reduction uses the squeeze film effect to create a lubricating layer of over-pressurized air between a fingertip and a vibrating surface, thus decreasing friction. The electroadhesive attraction method is based on a display surface in which an electrode layer is placed on top of a substrate and covered by an insulating layer. When the grounded fingertip touches the insulating layer, there is an electric field generated across the skin-surface interface. The electric field creates coulombic attraction and increases friction force.

However, since the electroadhesive friction and ultrasonic friction force are passive lateral forces and only resist the finger motion, they cannot assist in perception of shapes that would cause forces perpendicular to or in the same direction of movement [7]. Active lateral force feedback, therefore, is essential for virtual shape rendering.

Many interesting devices, such as stick-slip actuators and linear ultrasonic motors, have been developed to generate active lateral forces. The first piezoelectric stick-slip actuator was proposed by Anton L.O. Söderqvist in 1976 [10], followed by a great variety of such devices with advancements in flexure design, driving signals and control methods, as well as additional degrees of freedom. In general, the stick-slip actuator employs a sawtooth-waveform voltage as an input to produce a slow expansion and a quick contraction [11]–[13]. During the slow expansion, the actuator sticks to the load. During the quick contraction, it slips relative to the load due to a high inertia force. Cyclic slow expansion and fast contraction can produce a non-zero average force acting on the load [12], [14].

Linear ultrasonic motors employ out-of-plane elliptical oscillation to produce non-zero average forces on a load. They can be grouped into two categories: standing wave type and traveling wave type. Standing-wave motors feature a toothed stator that presses against the load (e.g., rotor) [15], [16]. By exciting different mode shapes of the stator, the standing-wave motor can control the direction of forcing. For traveling-wave actuators, three methods are used to generate elliptical oscillation, including impedance matching, two-mode excitation, and active sinking [17]–[20]. Even though the traveling wave actuator has a wider contact area than standing-wave actuators, it has lower electromechanical conversion efficiency, which leads to a low driving force [21].

Within the haptic field, researchers have created many devices to provide active lateral force feedback on the fingertip. Some of these use electric motors and articulated mechanical components to deliver the in-plane forces, which makes them difficult to apply to touchscreens where the expectation is no moving parts [22]–[24]. A tactile display proposed by Sofiane Ghenna et. al. employed an ultrasonic traveling wave to generate an active force on the finger, but was able to produce only a modest $\pm 100mN$ [25]. Motivated by the goal of achieving active lateral force feedback in a "solid state" device, our group

Manuscript received November 16, 2018; revised July 4, 2019; accepted August 7, 2019. Date of publication August 13, 2019; date of current version December 12, 2019. This paper was recommended for publication by Associate Editor F. Giraud upon evaluation of the reviewers' comments. This work was supported by the National Science Foundation under Grants IIS-1518602.
(Corresponding author: Heng Xu.)

The authors are with the Department of Mechanical Engineering, Northwestern University, Evanston, IL 60208-3111, USA (e-mail: hengxu@u.northwestern.edu; peshkin@northwestern.edu; colgate@northwestern.edu).
Digital Object Identifier 10.1109/TOH.2019.2934853

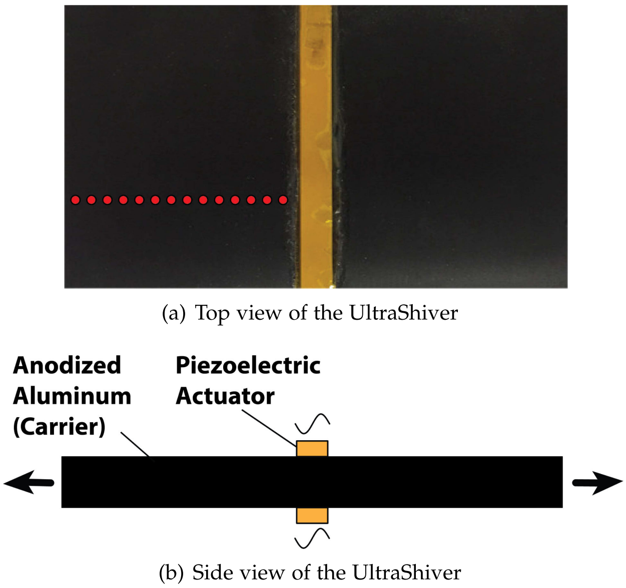

Fig. 1. The structure of the UltraShiver. The black block represents the anodized aluminum. The yellow block represents the piezoelectric actuator. The red dots represent points where velocity was measured in Section II-A3.

has studied lateral force feedback displays for ten years and we have developed a range of devices, including the ShiverPaD, the LateralPaD, and the eShiver [26]–[28].

The ShiverPaD consisted of a TPaD, a voice coil, and auxiliary structures [26]. The voice coil was used to oscillate the TPaD laterally. Over the course of part of an oscillation cycle, the friction was set low, and over the remainder of the cycle it was set high. This asymmetry enabled the ShiverPaD to generate a net lateral force in each cycle. One prototype was able to achieve around ± 100 mN lateral force at a vibratory frequency of 854 Hz [26]. The eShiver used a similar apparatus to provide in-plane motion [28]; however, it used electroadhesion ([9], [29], [30]) to modulate the friction force. The eShiver performed at a relatively low frequency of 55 Hz for an artificial finger and 1000 Hz for the human finger. It could generate a maximum lateral force of ± 450 mN on a human finger, making it more than strong enough for any envisioned use. A serious limitation of both the ShiverPaD and the eShiver was that they operated at audible frequencies.

To generate lateral force in the ultrasonic regime, the LateralPaD used piezoelectric actuators to drive normal and lateral resonances at the same ultrasonic frequency (22.3 KHz) [27]. Unlike the ShiverPaD and eShiver, the LateralPaD used a elliptical motion of the surface, similar to a traveling wave ultrasonic motor [31]. The LateralPaD could generate ± 50 mN, a force small enough that approximately 20% of people could not feel it during a demo session [32].

In this paper, we describe a new a haptic device, the UltraShiver, that can provide large lateral forces (± 400 mN) while operating in the ultrasonic regime (around 30 kHz). It oscillates an electroadhesive surface in-plane by using an ultrasonic longitudinal wave. The direction and magnitude of the lateral force can be adjusted by varying the phase between the in-plane oscillation and the electroadhesion. The UltraShiver makes it possible, for the first time, to apply large active lateral forces to a human fingertip in a solid state device, without audible artifact. A preliminary version of this paper has been published [33]. Here, we further include a lumped-parameter model (in Section IV-A), which is used to elucidate experimental results, and an example of active force feedback control (in Section IV-G).

II. Method and Experiments

A. Prototype Design and Analysis

1) UltraShiver Structure: The UltraShiver consists of a sheet of anodized aluminum excited in a compression-extension mode via piezoelectric actuators (Fig. 1). The anodized aluminum serves as an electroadhesive surface in which the aluminum layer is connected to a high voltage source and the anodized layer is an insulator.

The dimensions of the anodized aluminum are 84 mm $\times$ 60 mm $\times$ 1 mm. Two pieces of hard piezoceramic (SMPL60W5T03R112, Steminc and Martins Inc, Miami, FL, USA) are placed in the middle of the anodized aluminum. The two piezoelectric actuators are excited symmetrically, which exaggerates the oscillation in the in-plane direction and reduces the oscillation in the out-of-plane direction. Since the resonant frequency of the lateral oscillation depends on the Young's modulus, the density of the surface material, and the length of the surface in the lateral direction, the length of the surface was optimized to keep the resonant frequency of the lateral oscillation far from the resonant frequency of the normal oscillation, thus further decreasing the normal motion.

2) Finite Element Analysis: We simulated the motion of the UltraShiver using ABAQUS (ABAQUS Inc), which showed an extension-compression mode at the longitudinal resonance (in Fig. 2). There is only one nodal line in the middle of the anodized aluminum, which is parallel to the short edge of the anodized aluminum. Due to the symmetric motion of the two sides, we need to analyze the performance on only the left or right side of the piezoelectric actuator.

3) Velocity Profile Measurement: Since the oscillation of the surface is one of two fundamental features in the UltraShiver, it is necessary to characterize the velocity profile of the entire surface, including both lateral and normal components.

We measured the velocity at 14 points, all on the left side of the piezoelectric actuator (see Fig. 1(a)). These points ran parallel to the long side of the surface 20 mm from the edge, and were spaced 2.5 mm apart. The normal velocity was measured using a Laser Doppler Vibrometer (LDV). The lateral velocity was measured using a custom electromagnetic induction sensor, which was calibrated by the LDV. The UltraShiver was placed in a uniform magnetic field of 0.38 Tesla and a 5 mm long magnet wire was rigidly attached to each point, parallel to the short edge of the surface and perpendicular to the direction of the magnetic field. Lateral movement of the UltraShiver induced a voltage in each magnet wire. This voltage

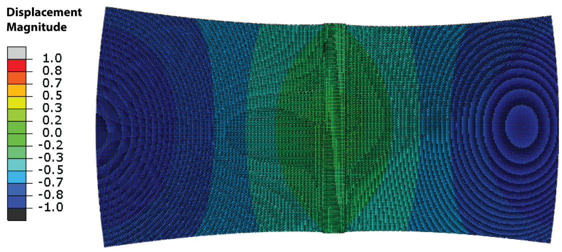

(a) Peak extension

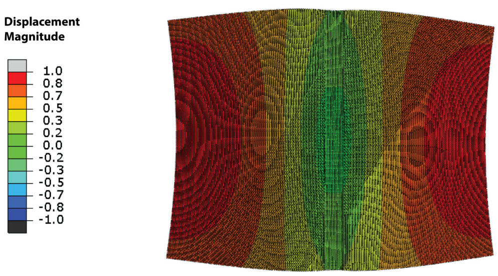

(b) Peak compression

Fig. 2. Finite element analysis of the UltraShiver. The displacement magnitude is normalized by its maximum value (6.32 μm).

was amplified and then recorded by an NI USB-6361. Each measurement was repeated five times.

B. Lateral Force Generation

The lateral force generation depends on the in-plane ultrasonic oscillation and the out-of-plane electroadhesive force, both operating at 30.1 kHz. The in-plane oscillation of the UltraShiver generates a lateral reaction force ($F_r = Z_l \upsilon_l$) on the fingertip, which is related to the fingertip's mechanical impedance in shear (Z_l) and the lateral velocity of the carrier (υ_l), assuming that the finger is stuck to the carrier. Stuck versus sliding is governed in part by the out-of-plane electroadhesive force ($F_e \propto {V_{gap}}^2$), which adjusts the friction force between the fingertip and the surface as a function of the gap voltage (V_{gap}) between the fingertip and surface [9], [29] (more details can be found in Section IV-A).

As illustrated in Fig. 3, the UltraShiver's operation can be divided into two phases within one period of in-plane vibration: a "push phase" and a "slip phase". In the "push phase", the gap voltage is set to a high value, compared to the "slip phase". The friction force (F_{push}) in the "push phase" is higher than that (F_{slip}) in the "slip phase", leading to a net pushing force.

There is a range of lateral velocities (υ_l) for which the lateral reaction force (F_r) is less than F_{push} and larger than the low friction force (F_{slip}) in the "slip phase". In this condition, the fingertip will slip in the "slip phase" and be stuck in the "push phase". The theoretical maximum net lateral force (F_{lf}) is equal to

$$F_{lf} = \frac{F_r - F_{slip}}{2} = \frac{Z_l \upsilon_l - F_{slip}}{2} \tag{1}$$

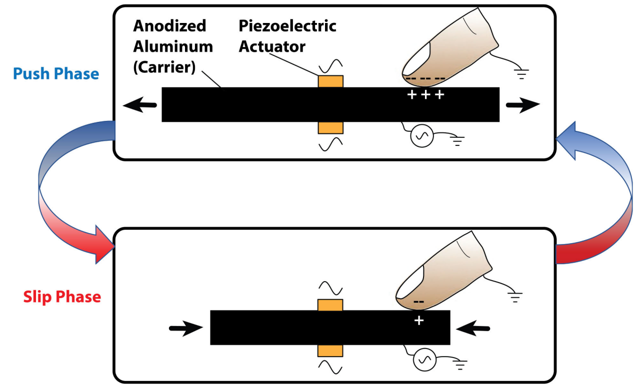

Fig. 3. Illustration of the lateral force generation in one period.

In this case, the net lateral force is sensitive to the relative carrier velocity (υ_l) and the gap voltage in the "slip phase".

When the carrier velocity (υ_l) is even higher, the lateral reaction force (F_r) can be larger than F_{push}. The fingertip then slips in both phases. In this case, the theoretical maximum net lateral force (F_{lf}) is equal to

$$F_{lf} = \frac{F_{push} - F_{slip}}{2} \tag{2}$$

In this situation, the net lateral force is sensitive to the gap voltage in the two phases.

When the relative carrier velocity (υ_l) is very low, the lateral reaction force (F_r) can be less than F_{slip}. Then the fingertip is stuck in both phases, and the net lateral force (F_{lf}) is equal to zero.

Thus, the UltraShiver can control the amplitude of the net lateral force by adjusting the amplitudes of the carrier velocity and the gap voltage. In addition, it can also change the direction of the net lateral force by adjusting the phase between the carrier velocity and the gap voltage.

In the UltraShiver, the voltage of piezoelectric actuators is used to control the carrier velocity of the surface. Even though the gap voltage (V_{gap}) is related to the electroadhesive force, it cannot be controlled directly. Instead, we control the total voltage (V_{total}) of the system (across the fingertip, the plate, and the air gap between them). Together with an electrical impedance measurement and an electrical model of the UltraShiver, we can estimate the voltage across the air gap. A detailed description of the electrical impedance model used in this study can be found in [9]. In addition, we assume that the total impedance of the system (Z_{total}) and the air gap impedance (Z_{gap}) do not change at a given ultrasonic frequency as the amplitude of the electroadhesive voltage changes. Thus, the gap voltage (V_{gap}) is equal to

$$V_{gap} = \frac{Z_{gap}}{Z_{total}} V_{total} \tag{3}$$

C. Experiments

Four experiments were performed to determine the relationship between lateral force and carrier velocity (υ_l), the total electroadhesive voltage (V_{total}), and the phase difference (θ)

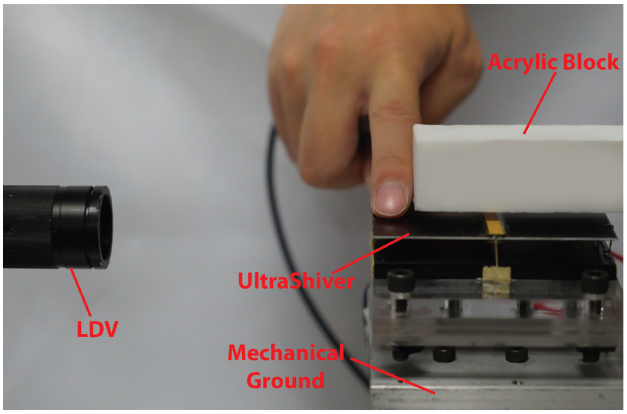

Fig. 4. Experiments platform.

between carrier velocity and electroadhesive voltage. Table I summarizes the parameters of electroadehsive voltages and piezoelectric voltages used in these four experiments in appendix V.

1) Experiment Setup: As shown in Fig. 4, the UltraShiver was mounted to mechanical ground with six brass flexures. A six-axis force sensor (ATI17 Nano load cell), which was placed underneath the UltraShiver, was used to measure lateral and normal forces. A Laser Doppler Vibrometer (LDV) was used to measure the carrier velocity at the end of the surface. The piezoelectric actuators were controlled with a piezoelectric amplifier outputting a sinusoidal signal at 30.1 kHz, and the electroadhesive voltage was modulated with a high voltage source (TREK 610C). Because the electroadhesion effect varies roughly as the square of the voltage, a DC offset was introduced to avoid frequency doubling. More details of the parameters are reported in each experiment.

During the experiments, the electrically grounded finger lightly touched the surface while pressing against an acrylic block to mechanically ground the rest of the finger (see Fig. 4). The interface area between the fingertip and the surface was close to the short edge of the surface, in order to acquire a high relative carrier velocity (shown in the Section III-A). All the signals were generated and recorded using an NI USB-6361 with a 200 kHz sampling frequency.

2) Experiment 1: Effect of Phase: This experiment was used to investigate the effect of the phase difference between the carrier velocity and the electroadhesive voltage. The voltage of piezoelectric actuators was set to 100 V peak-to-peak (at 30.1 kHz), which was chosen in the saturation range of the carrier velocity (more details are given in Sections IV-C and IV-D). The electroadhesive voltage was set to a sinusoidal voltage of peak amplitude 100 V and with an offset of 180 V. The frequency of the electroadhesive voltage (30.09 kHz) was set to 10 Hz less than that of the piezoelectric voltage, so that the phase between the carrier velocity and the electroadhesive voltage varied at 10 Hz. The subjects finger kept interacting with the device while the phase difference was varying. The experimental duration was 0.5 seconds.

3) Experiment 2: Effect of Carrier Velocity and Pressing Force: Even though the normal force was measured by the force sensor, the experimenter kept a constant pressing force (0.266 ± 0.027 N) as effectively as possible. The parameters of the electroadhesive voltage were the same as those in experiment 1. The voltage of piezoelectric actuators was randomly chosen from 4 V to 120 V peak-to-peak. Each measurement was repeated five times. The experimental duration for each trial was 1 second.

In addition, the experimenter repeated this experiment using a stronger pressing force (0.620 ± 0.041 N), in order to analyze the effect of different pressing forces on the lateral force.

4) Experiment 3: Effect of Electroadhesive Voltage: Since the electroadhesive voltage contains AC and DC components, the electroadhesive force (F_e) is represented as (together with Eq. (3)):

$$F_e \propto \left(\frac{Z_{gap}(f)}{Z_{total}(f)} V_{ACtotal} \sin(2\pi ft) + \frac{Z_{gap}(0)}{Z_{total}(0)} V_{DCtotal} \right)^2 \tag{4}$$

where f, $V_{ACtotal}$ and $V_{DCtotal}$ represent the frequency, the AC component magnitude, and the DC component of total voltage (V_{total}), respectively. In this experiment, the piezoelectric voltage was fixed at 100 V peak-to-peak, which was chosen in the saturation range of the carrier velocity (more details are given in Sections IV-D and IV-E). The value of $V_{ACtotal}$ was varied from 20 V to 150 V while the value of $V_{DCtotal}$ was set to 100 V, 150 V, or 200 V. Combinations of $V_{ACtotal}$ and $V_{DCtotal}$ were randomly chosen. Each combination was repeated five times. The experimental duration for each trial was 1 second.

5) Experiment 4: Effect of the Ratio of AC to DC Voltage: In this experiment, we defined a variable γ, the ratio of AC to DC voltage, as

$$\gamma = \frac{V_{ACtotal}}{V_{DCtotal}} \tag{5}$$

This experiment investigated the effect of this ratio γ on the lateral force under the same peak electroadhesive voltage.

$$V_{ACtotal} + V_{DCtotal} = 240 \text{ V} \tag{6}$$

γ was randomly chosen from 0.1 to 1.6 and measurements for each value were repeated five times. During each trial, the piezoelectric voltage was fixed at 100 V peak-to-peak, which was chosen in the saturation range of the carrier velocity (more details are given in Sections IV-D and IV-E). The experimental duration for each trial was 1 second.

III. Results

A. Vibration Velocity Profile

Fig. 5 shows the lateral and normal velocity on the left side of the surface. There is a large carrier velocity (1100 mm/s) at the edge of the surface. The carrier velocity decreases to 300 mm/s at the farthest-right measurement point, which is 8.25 mm from

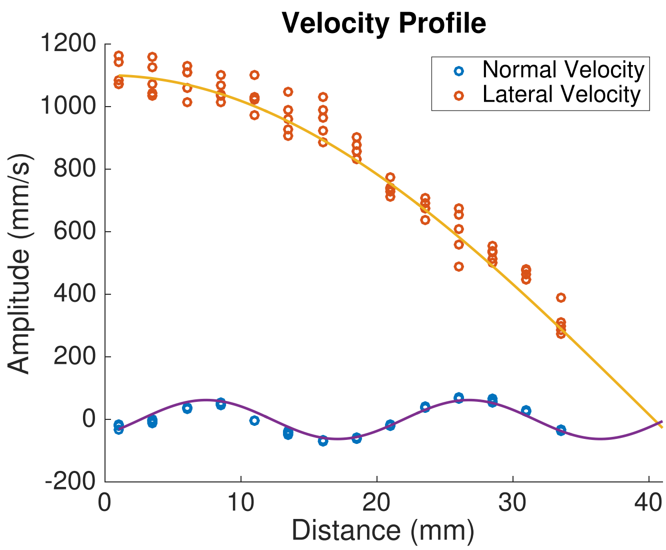

Fig. 5. Vibration velocity profile of the UltraShiver. The x axis represents the distance from a measurement point to the left short edge.

the center of the surface. There is only one longitudinal nodal line in the center, which matches the results of finite element analysis in Fig. 2. In addition, there is a normal oscillation with five nodal lines. The amplitude of the normal velocity is around 80 mm/s, which is 7% of the amplitude of the carrier velocity.

B. *Effect of Phase*

Fig. 6(a) shows the relation between the lateral force and the relative phase (i.e., the phase between carrier velocity and electroadhesive voltage). The maximum lateral force is achieved when the relative phase is equal to 0 or 180 degrees[1]. This means that the carrier velocity is optimally chosen to be in-phase or anti-phase with electroadhesive voltage.

C. *Effect of Carrier Velocity and Pressing Force*

Fig. 6(b) shows the relation between the carrier velocity and the lateral force under two different pressing forces. The carrier velocity changes from 100 mm/s to 1000 mm/s. The range of the lateral force varies from 0 to 0.35 N. In the case of low normal force, there are two turning points: when the carrier velocity is around 300 mm/s, and when it is around 700 mm/s. Before the carrier velocity reaches 300 mm/s, the UltraShiver cannot generate a net lateral force. When the carrier velocity increases from 300 mm/s to 700 mm/s, the lateral force increases significantly from 0.1 N to 0.35 N. When the carrier velocity increases from 700 mm/s to 1000 mm/s, the lateral force remains almost constant at 0.35 N.

As the pressing force increases, there is a similar velocity-force relation as that under a low force. There are still two turning points, but they shift slightly to around 400 mm/s and 820 mm/s. When the carrier velocity is in the range of 300 mm/s to 820 mm/s, the lateral force with a high pressing force is less than that with a low pressing force.

[1] Erroneous values reported in [33] have now been corrected for. The error resulted from a time delay in the velocity sensor.

D. *Effect of Electroadhesive Voltage*

Fig. 6(c) presents the relation between the peak amplitude of the AC voltage and the lateral force under different DC voltages. The maximum lateral force is around 0.4 N when the AC voltage ($V_{ACtotal}$) is 140 V and the DC voltage ($V_{DCtotal}$) is 200 V. Generally, the lateral force increases as a function of both AC voltage and DC voltage.

E. *Effect of the Ratio of AC to DC Voltage*

Fig. 6(d) shows the variation of lateral force with the ratio γ. Notably, there is a peak in lateral force when γ is about 0.55.

IV. Discussion

A. *Lumped-Parameter Model*

1) Model Assumptions and Principle: A lumped-parameter model was created to elucidate the dependence of lateral force on the carrier velocity, the electroadhesive voltage and the phase between them. In this model, we assume that the fingertip can switch between "stuck" and "sliding" (relative to the surface) within a small fraction of an oscillation cycle, which is supported by recent measurements showing bandwidth well into the ultrasonic regime [34]. Additionally, the results in Fig. 6(b) showing a smooth transition from zero to peak lateral force with increasing surface velocity suggest that friction switching is fast compared to the time scale of oscillation.

According to Fig. 6(a), peak force production occurs when the phase between the carrier velocity and the electroadhesive voltage is 0 or 180 degrees. This is consistent with the mechanical impedance of the fingertip being that of a pure damper (see further discussion in section 7.2). Thus, when the finger is stuck, the reaction force (F_r) is

$$F_r = B_{finger} \upsilon_l \tag{7}$$

The carrier velocity (υ_l) is a measured quantity, while the damping (B_{finger}) is a free parameter in the model.

The friction force between the fingertip and the surface depends on the sum of the electroadhesion force and the pressing force. Since the pressing force may affect the mechanical impedance of the fingertip as well as the contact area and the air gap thickness, parameters are fit for only a single (low) pressing force (0.266 ± 0.027 N), which was measured in the experiments (in Section II-C3). As we have reported previously [9], [29], the electroadhesion force (F_e) is equal to

$$F_e = \frac{A\varepsilon_0\varepsilon_{gap}}{2}\left(\frac{V_{gap}}{d_{gap}}\right)^2 \tag{8}$$

The gross contact area ($A = 30\ mm^2$) is taken from the work of Dzidek *et al.* [35]; ε_0 is the permittivity of free space; the dielectric constant of the gap is chosen to be that of air ($\varepsilon_{gap} = 1$); the voltage across the gap (V_{gap}) is calculated from the total voltage (V_{total}) and the electrical impedance of the gap (Z_{gap}) and the system (Z_{total}); and the static ($\mu_s = 0.5$)

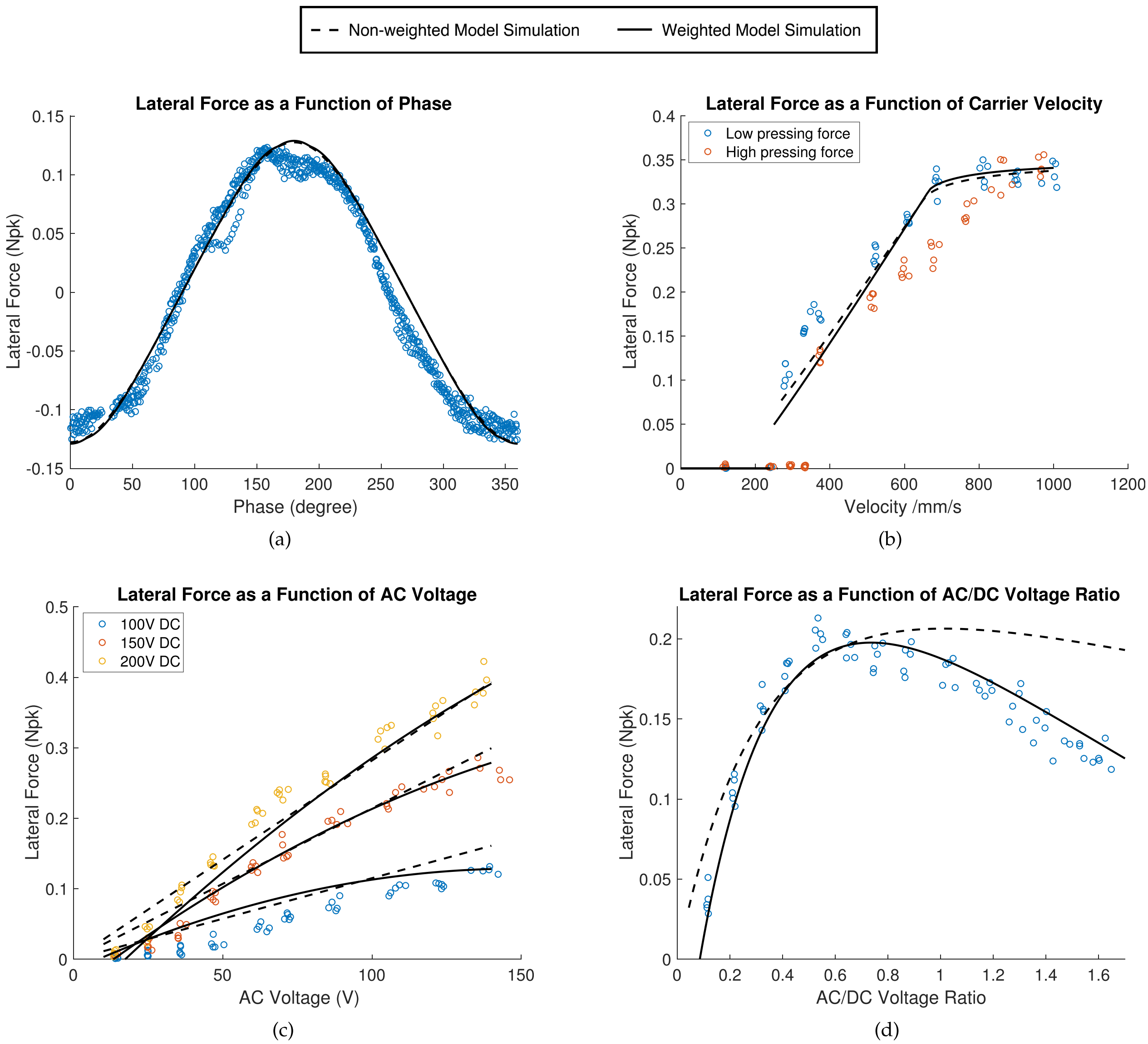

Fig. 6. Experiment results and model simulation. Each circle represents experiment data in one trial. The dashed lines are the model simulation without weighted electroadhesion force. The solid lines are the model simulation with weighted electroadhesion force. (a) Lateral force as a function of phase between the carrier velocity and the electroadhesive voltage. (b) Lateral force as a function of the carrier velocity underdifferent pressing forces. (c) Lateral force as a function of the AC component ofthe electroadhesive voltage under different DC components. (d) Lateral force as a function of ratio of AC to DCvoltage magnitudes.

and kinetic ($\mu_k = 0.25$) friction coefficients between the fingertip and the surface are taken from our previous study [9]. This leaves the thickness of the air gap between the fingertip and the surface (d_{gap}) as a free parameter.

Since the direction and the magnitude of static friction forces are modulated by the direction of the finger motion and electroadhesion, the static friction force is represented by the friction envelope (F_{fe}), shown in Fig. 7. When the friction envelope (F_{fe}) is larger than the reaction force (F_r), the fingertip remains stuck relative to the surface. In this case, the lateral force (F_{lf}) on the fingertip is equal to the reaction force (F_r). When the friction envelope (F_{fe}) is lower than the reaction force (F_r), the fingertip slips relative to the surface. In this case, the lateral force (F_{lf}) on the fingertip is equal to the friction force (F_{fe}). Averaged over a cycle, the lateral force generated on the fingertip is non-zero.

2) Model Simulation: The two free parameters (B_{finger} and d_{gap}) may be fit to our force-vs-velocity data, producing the results shown in Fig. 6(b). By using the MATLAB curve fitting toolbox, the best-fit values of B_{finger} and d_{gap} are 0.5 Ns/m and 2 μm, respectively, which are quite reasonable when compared to estimates in the literature [9], [36]. Other experimental data were also compared to the simulation with the results shown in Figs. 6(a), 6(c), and 6(d).

The model shows good agreement with the experimental results in most respects, but the predicted dependence on the AC/DC voltage ratio is clearly off. The optimal ratio is around 0.55 in the experiment results, but it is 1.00 in the simulation. The model and data diverge even more at higher values of the ratio.

3) Analytical Solution: Further insight into the effect of the AC to DC voltage ratio may be obtained if we make the

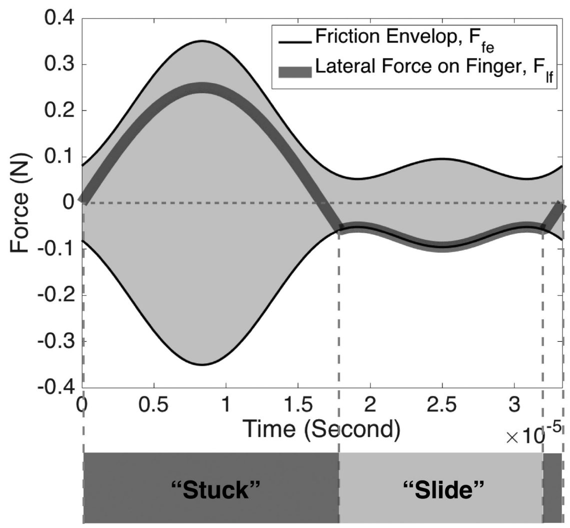

Fig. 7. Friction envelope and lateral force on the fingertip.

assumption that the surface velocity is high enough that the finger always slips, at both high and low friction levels. This is a reasonable assumption when we refer to the relation between the lateral force and the carrier velocity. In Fig. 6(b), when the finger lightly touches the surface and the carrier velocity is larger than 700 mm/s, the relation between the lateral force and the carrier velocity falls into the saturation zone (more details are shown in Section IV-D). That is also the reason why the carrier velocity was fixed at 1 m/s in Experiments 3 and 4. In this situation, the lateral force depends only on the sliding friction, and hence, electroadhesion force. The net lateral force (F_{lf}) may be estimated to be the averaged friction force over a cycle:

$$F_{lf} = \mu_k f \left[\int_0^{T/2} (F_p + F_e(t))dt - \int_{T/2}^{T} (F_p + F_e(t))dt \right] \tag{9}$$

where f is the frequency of the surface oscillation and F_p is the pressing force. Together with Eq. (8), the net lateral force (F_{lf}) is equal to

$$F_{lf} = F_1 - F_2 \tag{10}$$

Where F_1 and F_2 are

$$F_1 = \mu_k f \frac{A\varepsilon_0\varepsilon_{gap}}{2d_{gap}^2} \int_0^{T/2} (V_{DCgap} + V_{ACgap}\sin(2\pi ft))^2 dt \tag{11}$$

$$F_2 = \mu_k f \frac{A\varepsilon_0\varepsilon_{gap}}{2d_{gap}^2} \int_{T/2}^{T} (V_{DCgap} + V_{ACgap}\sin(2\pi ft))^2 dt \tag{12}$$

This works out to:

$$F_{lf} = \mu_k \frac{2A\varepsilon_0\varepsilon_{gap}}{d_{gap}^2} \frac{V_{ACgap}V_{DCgap}}{\pi} \tag{13}$$

where V_{DCgap} and V_{ACgap} represent the amplitude of DC voltage and AC voltage across the gap, respectively.

To build the connection between the lateral force (F_{lf}) and the ratio of AC to DC voltage (γ) in Eq. (13), some new notation is helpful:

$$V_{ACtotal} + V_{DCtotal} = V_{total} \tag{14}$$

$$\gamma = \frac{V_{ACtotal}}{V_{DCtotal}} \tag{15}$$

$$\lambda_{DC} = \frac{Z_{gap}(1\,\mathrm{Hz})}{Z_{total}(1\,\mathrm{Hz})} \tag{16}$$

$$\lambda_{AC} = \frac{Z_{gap}(30\,\mathrm{kHz})}{Z_{total}(30\,\mathrm{kHz})} \tag{17}$$

$V_{ACtotal}$, $V_{DCtotal}$, and V_{total} are the amplitudes of the AC voltage, DC voltage, and peak voltage across the system, respectively. $Z_{gap}(1\,\mathrm{Hz})$, $Z_{total}(1\,\mathrm{Hz})$, $Z_{gap}(30\,\mathrm{kHz})$, and $Z_{total}(30\,\mathrm{kHz})$ are the DC impedance of the gap, the DC impedance of the system, the AC impedance of gap, the AC impedance of the system, which are measured in preliminary experiments. Thus, the DC and AC voltage across the gap can be represented as

$$V_{DCtotal} = \frac{V_{total}\lambda_{DC}}{1+\gamma} \tag{18}$$

$$V_{ACtotal} = \frac{\gamma V_{total}\lambda_{AC}}{1+\gamma} \tag{19}$$

Combining Eq. (13) with Eqs. (18) and (19), the net lateral force can be simplified as

$$F_{lf} = \mu_k \frac{2A\varepsilon_0\varepsilon_{gap}}{d_{gap}^2} \frac{\lambda_{DC}\lambda_{AC}V_{total}^2}{\pi} \frac{\gamma}{(1+\gamma)^2} \tag{20}$$

This result predicts that, when the ratio (γ) is equal to 1, there is a maximum lateral force. This is consistent with the simulation and not the experimental results. In addition, it should be noted that the maximum is independent of electrical impedance of the gap and the system.

4) Analytical Solution With Weighted Electroadhesion Force: A possible explanation of the discrepancy is found in our previous study [34], which showed that the relation between electroadhesion force and the gap voltage does not always follow the square law from Eq. (8). For surfaces with diamond-like coating (DLC), the electroadhesion force quickly saturates when the command current is larger than 1 mA pk [34]. Even though the reason behind this saturation is still unclear, one possible speculation is the low roughness of the surface. Such lateral force saturation with a high electrical input could be a reason why the model fails to accurately predict the relation between the lateral force and the ratio of AC to DC voltage.

Thus, effects of the lateral force saturation are included in an improved model by introducing two weight factors (α and β) for high and low electroadhesive voltage. Eqs. (10), (13) and (20) are updated to Eqs. (21), (22) and (23).

$$F_{lf} = \alpha F_1 - \beta F_2 \tag{21}$$

$$F_{lf} = \mu_k \frac{A\varepsilon_0\varepsilon_{gap}}{2d_{gap}^2}\left[\frac{2V_{DCgap}^2 + V_{ACgap}^2}{4}(\alpha-\beta) + \frac{2V_{ACgap}V_{DCgap}}{\pi}(\alpha+\beta)\right] \tag{22}$$

$$F_{lf} = \mu_k \frac{A\varepsilon_0\varepsilon_{gap}V_{total}^2}{2d_{gap}^2(1+\gamma)^2}\left[\frac{2\lambda_{DC}^2 + \gamma^2\lambda_{AC}^2}{4}(\alpha-\beta) + \frac{2\lambda_{DC}\lambda_{AC}\gamma}{\pi}(\alpha+\beta)\right] \tag{23}$$

When β is assumed to be 1, there are two free parameters in the improved model, including the high voltage weight factor (α) and the thickness of the gap (d_{gap}). The improved model with weighted electroadhesion force is fit to our force-vs-ratio data (shown in Fig. 6(d)). The best-fit (R-square = 0.881) values of α and d_{gap} are 0.5318 and 1.42 μm, respectively, which fall into a reasonable range [9]. The high voltage weight factor (α = 0.5318) is less than the low voltage weight factor (β = 1), which is consistent with our observation of the high electrical source saturation [34].

The improved model with updated weight factors (α and β) and gap thickness (d_{gap}) is fit to our force-vs-velocity data for a single (low) pressing force. In this fit, there is only one free parameter: the mechanical damping of the fingertip (B_{finger}). The fitting result is shown in Fig. 6(b). The best-fit value of B_{finger} is 0.54 Ns/m, which also falls into a reasonable range [36]. Other experimental data were also compared to simulation with the results shown in Figs. 6(a) and 6(c), which show good agreement with the experimental results.

B. Vibration Velocity Profile

Even though the UltraShiver is intended to generate longitudinal motion only, the velocity profile data show that there is still a small amount of normal motion. This may be due to imperfections in the fabrication of the UltraShiver: the relative position of the piezoelectric actuators on the anodized aluminum is manually adjusted, and the actuators may not be placed exactly symmetrically. Alternatively, the electrical and mechanical properties of the two actuators may not be exactly the same. Either reason would lead to non-zero normal motion. Fortunately, the normal motion is small compared to the lateral motion. The rest of experiments also suggest that the normal motion does not affect the lateral force generation or the control of its direction.

C. Effect of Phase

Fig. 6(a) shows a near-sinusoidal dependence of the lateral force on the phase between carrier velocity and electroadhesive voltage. Those data were taken with a carrier velocity of about 1000 mm/s ensuring that the lateral force stayed in the saturation zone (more details are given in Section IV-D). The analytical solution presented in section 6.3 also made the assumption of high carrier velocity, but did not include a variable phase. It is straight forward to include that phase, resulting in a modified solution for lateral force:

$$F_{lf} = -\mu_k \frac{2A\varepsilon_0\varepsilon_{gap}}{d_{gap}^2}\frac{V_{ACgap}V_{DCgap}}{\pi}\cos(\varphi) \tag{24}$$

The sinusoidal dependence on phase is now apparent. This result also predicts maximum lateral force when φ is equal to 0 or 180 degrees which is consistent with the results in Fig. 6(a). This suggests that the slip velocity, upon which friction depends, is in-phase with the carrier velocity. This in turn suggests that the lateral velocity of the skin is in-phase with the friction force. We conclude that the viscosity of the fingertip (as opposed to stiffness or mass) dominates its shear impedance. Both the reasonable simulated damping and the good predictions of the model support this assumption. However, an in-depth explanation of these results should be derived from measurements of the mechanical and electrical impedance, which are aspects of our ongoing work.

D. Effect of Carrier Velocity and Pressing Force

The relation between the carrier velocity and the lateral force can be divided into three zones, including the stuck zone, the linear zone, and the saturation zone.

In the stuck zone, the reaction force (F_r) from the relative carrier velocity (υ_l) is less than the low friction force (F_{slide}). The fingertip is always stuck during the back-forth motion of the surface. In this zone, the UltraShiver cannot generate the lateral force. As shown in Fig. 6(b), when the finger lightly touches the surface and the carrier velocity is less than 300 mm/s, the interaction between the fingertip and the UltraShiver falls into the stuck zone.

In the linear zone, the reaction force (F_r) is less than the high friction force (F_{stuck}) and larger than the low friction force (F_{slide}). The fingertip will slide in one direction and get stuck in another direction. According to Eq. (1), there is a linear relation between the carrier velocity and the lateral force for a given electroadhesive voltage. As shown in Fig. 6(b), when the finger lightly touches the surface and the carrier velocity varies from 300 mm/s to 700 mm/s, the interaction between the fingertip and the UltraShiver falls into the linear zone.

In the saturation zone, the reaction force (F_r) is larger than the high friction force (F_{stuck}). The fingertip slides in both directions. Based on Eq. (2), the lateral force is close to constant in this zone for a given electroadhesive voltage. Thus, this zone presents a saturating relation between the carrier velocity and lateral force. As shown in Fig. 6(b), when the finger lightly touches the surface and the carrier velocity is larger than 700 mm/s, the interaction between the fingertip and the UltraShiver falls into the saturation zone.

In addition, as we increase the pressing force, the friction force also increases. Even though there are still the three zones, the UltraShiver needs more carrier velocity to produce

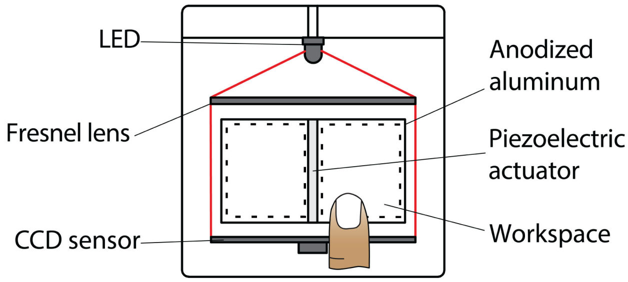

Fig. 8. Platform of the potential well application.

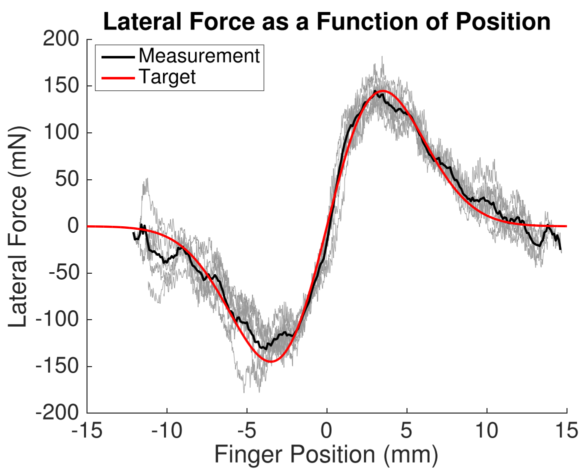

Fig. 9. Potential well: lateral force as a function of finger position. The gray curves are recorded in five trials. The black curve is the average of the five trials. The red curve is the target of this rendering.

a reaction force that will cause sliding. Thus, the carrier velocity associated with the two turning points will shift to higher values.

E. Effect of Electroadhesive Voltage

When testing the effect of electroadhesive voltage, the carrier velocity was set to a high value of about 1000 mm/s. This ensured that the lateral force stayed in the saturation zone (sliding in both directions). In saturation, we would expect an increase in either AC or DC voltage to increase lateral force (see Eqs. (2) and (4)). The data show precisely this for the selected electroadhesive voltage range. Based on the model, it is worth noting that the positive correlation between the lateral force and the electroadhesive voltage is not always true. Eq. (22) shows that if $V_{DCgap} \gg V_{ACgap}$ (or $V_{ACgap} \gg V_{DCgap}$), the lateral force decreases when the AC or DC voltage increases, due to the electroadhesion force providing less bias in one oscillation cycle under the condition where $V_{DCgap} \gg V_{ACgap}$ (or $V_{ACgap} \gg V_{DCgap}$).

F. Effect of the Ratio of AC to DC Voltage

This experiment was also performed at a carrier velocity of about 1000 mm/s ensuring operation in the saturation zone. Two factors motivated our interest in the optimal ratio of AC to DC voltage. First, the electroadhesion force varies, roughly speaking, as the square of the gap voltage. Because of the square law dependence, it is necessary to minimize the absolute value of the gap voltage during the sliding phase. To accomplish this, the zero-mean AC component is offset by a DC component. The second consideration is that the transfer function relating applied voltage to gap voltage is frequency dependent, which means that the AC and DC components of the gap voltage will not be identical to those of the applied waveform. Thus, it is not sufficient merely to select equal DC and AC magnitudes ($\gamma = 1$). Indeed, as the data show, peak force occurs near $\gamma = 0.55$, suggesting one of two explanations. First, it may be that DC gap voltage is attenuated more than AC gap voltage. This may be due to "leakage" through the stratum corneum [37]. Alternatively, the electroadhesion force may saturate at high values of electrical input, as suggested by Shultz's model [34].

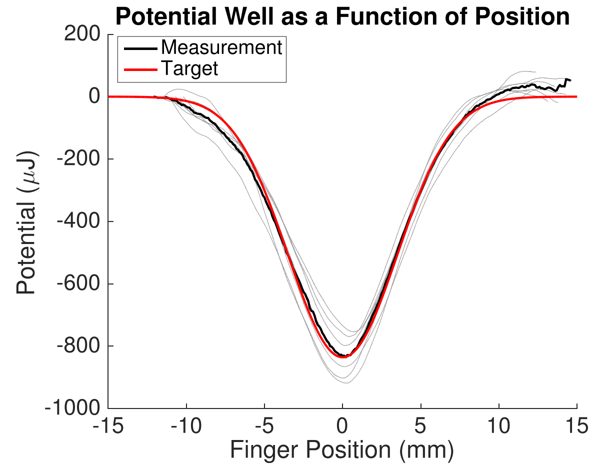

Fig. 10. Potential well: Potential as a function of finger position. The gray curves are integrated from force measurements in five trials. The black curve is the average of the five trials. The red curve is the target of this rendering.

G. Example of Force Feedback

As a controllable lateral force source, the UltraShiver is used to render haptic features on the surface via integration with a finger position sensor (shown in Fig. 8). The finger position sensor consists of a CCD sensor (TSL1412s, AMS-TAOs Inc.) and a Fresnel lens. The CCD sensor uses an array of 1536 photodiodes with an 8 μm resolution and an 8.3 kHz update rate. The Fresnel lens is used to generate a parallel light and cover the whole workspace of the UltraShiver. In this paper, we show a Gaussian-like potential well rendering as an example.

1) Gradient-Based Lateral Force Control Algorithm: The rendering algorithm is based on the gradient of Gaussian-like potential well, which has been widely used by researchers in this field [6], [7]. Since the UltraShiver is an active lateral force source, it can assist and resist the finger movement. The positive and negative maximum gradient are linearly mapped to the positive and negative maximum lateral force. The input of the algorithm is the finger position, and the output is the

TABLE I
PARAMETERS OF ELECTROADHESIVE VOLTAGES AND PIEZOELECTRIC VOLTAGES USED IN EXPERIMENTS 1-4

Experiment	Piezoelectric Voltage		Electroadhesion Voltage		
	Amplitude (V pk-pk)	Frequency (kHz)	Amplitude DC (V)	Amplitude AC (V pk)	Frequency (kHz)
#1	100	30.1	180	100	30.09
#2	4-120	30.1	180	100	30.09
#3	100	30.1	100, 150, 200	20-150	30.09
#4	100	30.1	AC + DC = 240		30.09

phase between the carrier velocity and the electroadhesive voltage, which is based on the results in Fig. 6(a). The update rate of the potential well rendering is 8.3 kHz.

2) Lateral Force and Shape Profile: The lateral force was recorded while the finger was passively interacting with the potential well. The scanning speed of the finger was 60 mm/s. Fig. 9 shows the lateral force as a function of the finger position in five trials. In addition, the lateral force measurements were integrated to illustrate the relation between the potential and the finger position (in Fig. 10). Both the lateral force and potential results show that the UltraShiver has good ability to control the active lateral force.

V. CONCLUSION & FUTURE WORK

The UltraShiver, which can generate a strong lateral force (400 mN) with silent operation, is a simple and robust device that should serve as the basis for a wide variety of bare finger force feedback applications. Both the experimental results and the model simulation show the influences of carrier velocity, electroadhesive voltage, and the phase between them, on the lateral force. Once integrated with finger position sensing, the UltraShiver may be used to render haptic features.

Since the saturation of the electroadhesion force at high voltage has been reported for only the DLC coating surface, it will be necessary to look for a similar saturation in the context of the anodized aluminum surface used here. This will be necessary to verify the assumptions in Section IV-A4. In addition, the experiments reported here will be conducted with more subjects to examine inter-subject variability. Finally, extension of the technique to two in-plane axes and integration with force sensing will be explored.

APPENDIX A
SUMMARY OF EXPERIMENTAL PARAMETERS

The electroadhesive and piezoelectric voltages used in Experiments 1-4 are shown in Table I.

ACKNOWLEDGEMENT

The assistance of R. F. Friesen in editing this manuscript is gratefully acknowledged.

REFERENCES

[1] T. Watanabe and S. Fukui, "A method for controlling tactile sensation of surface roughness using ultrasonic vibration," in *Proc. 1995. IEEE Int. Conf. Robot. Autom.*, 1995, vol. 1, pp. 1134–1139.

[2] J. Linjama and V. Mäkinen, "E-sense screen: Novel haptic display with capacitive electrosensory interface," in *Proc. 4th Workshop Haptic Audio Interact. Des.*, 2009, pp. 10–11.

[3] O. Bau, I. Poupyrev, A. Israr, and C. Harrison, "Teslatouch: electrovibration for touch surfaces," in *Proc. 23nd Annu. ACM Symp. User Interface Softw. Technol.*, 2010, pp. 283–292.

[4] D. J. Meyer, M. Wiertlewski, M. A. Peshkin, and J. E. Colgate, "Dynamics of ultrasonic and electrostatic friction modulation for rendering texture on haptic surfaces." in *Proc. IEEE Haptics Symp.*, 2014, pp. 63–67.

[5] S. Saga and K. Deguchi, "Lateral-force-based 2.5-dimensional tactile display for touch screen," in *Proc. IEEE Haptics Symp.*, 2012, pp. 15–22.

[6] S.-C. Kim, A. Israr, and I. Poupyrev, "Tactile rendering of 3D features on touch surfaces," in *Proc. 26th Annu. ACM Symp. User Interface Softw. Technol.*, 2013, pp. 531–538.

[7] R. H. Osgouei, J. R. Kim, and S. Choi, "Improving 3D shape recognition with electrostatic friction display," *IEEE Trans. Haptics*, vol. 10, no. 4, pp. 533–544, Oct.–Dec. 2017.

[8] L. Winfield, J. Glassmire, J. E. Colgate, and M. Peshkin, "T-pad: Tactile pattern display through variable friction reduction," in *Proc. 2nd Joint EuroHaptics Conf. Symp. Haptic Interfaces Virtual Environ. Teleoperator Syst.*, 2007, pp. 421–426.

[9] C. D. Shultz, M. A. Peshkin, and J. E. Colgate, "Surface haptics via electroadhesion: Expanding electrovibration with Johnsen and Rahbek," in *Proc. World Haptics Conf.*, 2015, pp. 57–62.

[10] A. L. Soderqvist, "Method and device for displacement of a workpiece," U.S. Patent 3,957,162, May 18, 1976.

[11] T. Takano, Y. Tomikawa, M. Aoyagi, and C. Kusakabe, "Piezoelectric actuators driven by the saw-tooth-like motion of a stator," *Ultrasonics*, vol. 34, no. 2–5, pp. 279–282, 1996.

[12] J. Peng and X. Chen, "Modeling of piezoelectric-driven stick–slip actuators," *IEEE/ASME Trans. Mechatronics*, vol. 16, no. 2, pp. 394–399, Apr. 2011.

[13] P. Pan, F. Yang, Z. Wang, B. Zhong, L. Sun, and C. Ru, "A review of stick–slip nanopositioning actuators," in *Nanopositioning Technologies*. Berlin, Germany: Springer, 2016, pp. 1–32.

[14] D. Karnopp, "Computer simulation of stick-slip friction in mechanical dynamic systems," *J. Dyn. Syst., Meas. Control*, vol. 107, no. 1, pp. 100–103, 1985.

[15] O. Vyshnevsky, S. Kovalev, and W. Wischnewskiy, "A novel, single-mode piezoceramic plate actuator for ultrasonic linear motors," *IEEE Trans. Ultrasonics, Ferroelectrics, Frequency Control*, vol. 52, no. 11, pp. 2047–2053, Nov. 2005.

[16] S. He, W. Chen, X. Tao, and Z. Chen, "Standing wave bi-directional linearly moving ultrasonic motor," *IEEE Trans. Ultrasonics, Ferroelectrics, Frequency Control*, vol. 45, no. 5, pp. 1133–1139, Sep. 1998.

[17] M. Kuribayashi, S. Ueha, and E. Mori, "Excitation conditions of flexural traveling waves for a reversible ultrasonic linear motor," *J. Acoust. Soc. Amer.*, vol. 77, no. 4, pp. 1431–1435, 1985.

[18] Y. Tomikawa, K. Adachi, H. Hirata, T. Suzuki, and T. Takano, "Excitation of a progressive wave in a flexurally vibrating transmission medium," *Japanese J. Appl. Phys.*, vol. 29, no. S1, p. 179, 1990.

[19] N. Tanaka and Y. Kikushima, "Active wave control of a flexible beam: Proposition of the active sink method," *JSME Int. J. Ser. 3, Vibration, Control Eng., Eng. Ind.*, vol. 34, no. 2, pp. 159–167, 1991.

[20] A. Minikes, R. Gabay, I. Bucher, and M. Feldman, "On the sensing and tuning of progressive structural vibration waves," *IEEE Trans. Ultrasonics, Ferroelectrics Frequency Control*, vol. 52, no. 9, pp. 1565–1576, Sep. 2005.

[21] S. Kondo, D. Koyama, and K. Nakamura, "Miniaturization of the traveling wave ultrasonic linear motor using series connection of bimorph transducers," in *Proc. IEEE Int. Ultrasonics Symp.*, 2011, pp. 790–793.

[22] J. Mullenbach, D. Johnson, J. E. Colgate, and M. A. Peshkin, "Activepad surface haptic device," in *Proc. IEEE Haptics Symp.*, 2012, pp. 407–414.

[23] S. Saga and R. Raskar, "Simultaneous geometry and texture display based on lateral force for touchscreen," in *Proc. World Haptics Conf.*, 2013, pp. 437–442.

[24] Force Dimension, "Omega.7," [Online]. Available: http://www.forcedimension.com/products/omega-7/overview

[25] S. Ghenna, E. Vezzoli, C. Giraud-Audine, F. Giraud, M. Amberg, and B. Lemaire-Semail, "Enhancing variable friction tactile display using an ultrasonic travelling wave," *IEEE Trans. Haptics*, vol. 10, no. 2, pp. 296–301, Apr.–Jun. 2017.

[26] E. C. Chubb, J. E. Colgate, and M. A. Peshkin, "ShiverPaD: A glass haptic surface that produces shear force on a bare finger," *IEEE Trans. Haptics*, vol. 3, no. 3, pp. 189–198, Jul.-Sep. 2010.

[27] X. Dai, J. E. Colgate, and M. A. Peshkin, "LateralPaD: A surface-haptic device that produces lateral forces on a bare finger," in *Proc. IEEE Haptics Symp.*, 2012, pp. 7–14.

[28] J. Mullenbach, M. Peshkin, and J. E. Colgate, "eShiver: Lateral force feedback on fingertips through oscillatory motion of an electroadhesive surface," *IEEE Trans. Haptics*, vol. 10, no. 3, pp. 358–370, Jul.-Sep. 2016.

[29] A. Johnsen and K. Rahbek, "A physical phenomenon and its applications to telegraphy, telephony, etc.," *J. Inst. Elect. Eng.*, vol. 61, no. 320, pp. 713–725, 1923.

[30] U. A. Alma, G. Ilkhani, and E. Samur, "On generation of active feedback with electrostatic attraction," in *Proc. Int. Conf. Human Haptic Sens. Touch Enabled Comput. Appl.*, 2016, pp. 449–458.

[31] N. W. Hagood and A. J. McFarland, "Modeling of a piezoelectric rotary ultrasonic motor," *IEEE Trans. Ultrasonics, Ferroelectrics, Frequency Control*, vol. 42, no. 2, pp. 210–224, Mar. 1995.

[32] J. M. Mullenbach, "Force feedback on the fingertip: Creating a surface haptic display through oscillation of an electroadhesive surface," Ph.D. dissertation, Department of Mechanical Engineering, Northwestern Univ., 2016.

[33] H. Xu, M. A. Peshkin, and J. E. Colgate, "Ultrashiver: Lateral force feedback on a bare fingertip via ultrasonic oscillation and electroadhesion," in *Proc. IEEE Haptics Symp.*, 2018, pp. 198–203.

[34] C. Shultz, E. Colgate, and M. A. Peshkin, "The application of tactile, audible, and ultrasonic forces to human fingertips using broadband electroadhesion," *IEEE Trans. Haptics*, vol. 11, no. 2, pp. 279–290, Apr.–Jun. 2018.

[35] B. M. Dzidek, M. J. Adams, J. W. Andrews, Z. Zhang, and S. A. Johnson, "Contact mechanics of the human finger pad under compressive loads," *J. Roy. Soc. Interface*, vol. 14, no. 127, 2017, Art. no. 20160935.

[36] M. Wiertlewski and V. Hayward, "Mechanical behavior of the fingertip in the range of frequencies and displacements relevant to touch," *J. Biomechanics*, vol. 45, no. 11, pp. 1869–1874, 2012.

[37] D. J. Meyer, M. A. Peshkin, and J. E. Colgate, "Fingertip friction modulation due to electrostatic attraction," in *Proc. World Haptics Conf.*, 2013, pp. 43–48.

Heng Xu is currently working toward the Ph.D. degree with the Department of Mechanical Engineering, Northwestern University, Evanston, IL, USA. His research interests include surface haptics, electrotactile stimulation, and tactile sensory feedback.

Michael A. Peshkin is currently the Bette and Neison Harris Professor of Teaching Excellence with the Department of Mechanical Engineering, Northwestern University, Evanston, IL, USA. His research interests include haptics, robotics, human–machine interaction, and rehabilitation robotics. He has co-founded four start-up companies: Mako Surgical, Cobotics, HDT Robotics, and Tanvas. He is a Fellow of the National Academy of Inventors, and (with J. E. Colgate) an inventor of cobots.

J. Edward Colgate is currently the Breed University Design Professor with Northwestern University, Evanston, IL, USA. He is known for his work in haptics and human–robot collaboration. He was an Associate Editor for the IEEE TRANSACTIONS ON ROBOTICS AND AUTOMATION, and the founding Editor-in-Chief of the IEEE TRANSACTIONS ON HAPTICS. He was one of the founding Co-Directors of the Segal Design Institute, Northwestern University. He has founded three start-up companies where the most recent of which, Tanvas, Inc., is commercializing an innovative haptic touch screen. He is a Fellow of the National Academy of Inventors.